Princeton Plasma Physics Laboratory

PPPL- 5104

PPPL-5104

Extending the Physics Basis of Quiescent H-mode toward ITER Relevant Parameters

W.M. Solomon, K.H. Burrell, M.E. Fenstermacher, A.M. Garofalo,
B.A. Grierson, A. Loarte, G.R. McKee, R. Nazikian, and P.B. Snyder

December 2014

Prepared for the U.S. Department of Energy under Contract DE-AC02-09CH11466.

Princeton Plasma Physics Laboratory
Report Disclaimers

Full Legal Disclaimer

Trademark Disclaimer

PPPL Report Availability

Princeton Plasma Physics Laboratory:

http://www.pppl.gov/techreports.cfm

Office of Scientific and Technical Information (OSTI):

http://www.osti.gov/scitech/

Related Links:

U.S. Department of Energy

Office of Scientific and Technical Information

Extending the Physics Basis of Quiescent H-mode toward ITER Relevant Parameters

W.M. Solomon[1], K.H. Burrell[2], M.E. Fenstermacher[3], A.M. Garofalo[2], B.A. Grierson[1], A. Loarte[4], G.R. McKee[5], R. Nazikian[1], and P.B. Snyder[2]

[1]Princeton Plasma Physics Laboratory, Princeton, New Jersey 08543-0451, USA
[2]General Atomics, San Diego, California 92186-5608, USA
[3]Lawrence Livermore National Laboratory, Livermore, California 94551, USA
[4]ITER Organization, Route de Vinon sur Verdon, 13115 St Paul Lez Durance, France
[5]University of Wisconsin-Madison, Madison, Wisconsin 53706, USA

E-mail: wsolomon@pppl.gov

Abstract. Recent experiments on DIII-D have overcome a long-standing limitation in accessing quiescent H-mode (QH-mode), a high confinement state of the plasma that does not exhibit the explosive instabilities associated with edge localized modes (ELMs). In the past, QH-mode was associated with low density operation, but has now been extended to high normalized densities compatible with operation envisioned for ITER. Through the use of strong shaping, QH-mode plasmas have been maintained at high densities, both absolute ($\bar{n}_e \approx 7 \times 10^{19}$ m^{-3}) and normalized Greenwald fraction ($\bar{n}_e/n_G > 0.7$) . In these plasmas, the pedestal can evolve to very high pressures and current as the density is increased. Calculations of the pedestal height and width from the EPED model are quantitatively consistent with the experimental observed evolution with density. The comparison of the dependence of the maximum density threshold for QH-mode with plasma shape help validate the underlying theoretical peeling-ballooning models describing ELM stability. High density QH-mode operation with strong shaping has allowed stable access to a previously predicted regime of very high pedestal dubbed "Super H-mode". In general, QH-mode is found to achieve ELM-stable operation while maintaining adequate impurity exhaust, due to the enhanced impurity transport from an edge harmonic oscillation, thought to be a saturated kink-peeling mode driven by rotation shear. In addition, the impurity confinement time is not affected by rotation, even though the energy confinement time and measured shear is observed to increase at low toroidal rotation. Together with demonstrations of high beta, high confinement and low q_{95} for many energy confinement times, these results suggest QH-mode as a potentially attractive operating scenario for ITER's Q=10 mission.

PACS numbers: 52.55.Fa, 52.25.Fi, 52.30.Cv, 52.55.Tn

1. Introduction

Future burning plasma devices such as ITER [1] are typically designed assuming H-mode levels of confinement, but require a plasma edge regime that keeps divertor heat loads to an acceptable level. However, standard H-mode is associated with steep gradients in the plasma edge forming the so-called pedestal, and these strong gradients are observed to trigger edge localized modes (ELMs) [2], resulting from exceeding the peeling-ballooning stability limit. Although ELMs prevent impurity accumulation in the core, they may lead to unacceptable divertor heat loads in a device such as ITER [3]. As such, significant effort is being spent to investigate external means of either eliminating or at least reducing the heat fluxes from ELMs, all while retaining the positive benefits of impurity flushing and without compromising the pedestal height.

An ideal solution to eliminating ELMs is to utilize scenarios that are peeling-ballooning stable, but which still possess good H-mode confinement, such as Quiescent H-mode (QH-mode) [4] or I-mode [5]. In QH-mode, the transport associated with ELMs is replaced by a benign "edge harmonic oscillation" (EHO) [4], or in some cases a more broadband form of MHD, which limits the plasma to just below the peeling-ballooning stability limit. The following sections cover recent advances in qualifying QH-mode as a possible operating scenario to meet ITER's $Q = 10$ mission.

2. High normalized fusion performance in QH-mode

Recent experiments have extended QH-mode to high normalized fusion performance, $G = \beta_N H_{89}/q_{95}^2 \approx 0.36$ approaching the level required for $Q = 10$ performance on ITER ($G \approx 0.42$), with values for the confinement factor H_{89}, β_N and q_{95} sustained at ITER relevant values for many energy confinement times in an ITER similar shape, as shown in Fig. 1.

To date, these results have been achieved in plasmas with significant counter neutral beam injection (NBI) torque. As reported previously, the confinement in QH-mode is actually found to increase as the torque and rotation is reduced toward balanced torque injection [6], so one anticipates that these results may be significantly improved at low torque. In general, QH-mode operation is maintained at low neutral beam torque through the use of non-axisymmetric fields, which has been found to drive the plasma toward the neoclassical "offset" rotation in the counter-I_p direction [7]. This enables the edge rotation shear, believed important for QH-mode operation, to be maintained in the absence of neutral beam torque. Nonetheless, even with strong $n = 3$ non-axisymmetric fields, efforts to investigate high G operation at low torque have been hampered by locked modes observed at lower q_{95}. In particular, while QH-mode is robustly maintained at

$\beta_N \approx 2$ through zero torque at $q_{95} \gtrsim 4.5$ with the use of $n = 3$ non-axisymmetric fields, increasing levels of (counter) NBI torque have been required to avoid locked modes as q_{95} is reduced, and at $q_{95} \approx 3.3$ it has proven difficult to reduce the torque below about 2 Nm, as can be seen in Fig. 2.

Separately, experiments have tried to investigate the viability of *accessing* QH-mode with low torque, since an outstanding question is whether non-axisymmetric fields can initiate the conditions for QH-mode without first spinning the plasma with counter NBI torque. Encouragingly, Fig. 3 shows that access to QH-mode at very low NBI torque may be achievable. In this example with $q_{95} > 4.5$, the L-H transition occurs around 1670 ms, followed by standard ELM-free H-mode. The internal coil begins ramping up an $n = 3$ field beginning at 1780 ms, and the first ELM occurs before the coils reach their programmed maximum. Following this one ELM, the plasma begins to exhibit weak broadband MHD activity characteristic of QH-mode, ELMs are absent and the density becomes better regulated. During this period lasting approximately 200 ms, the plasma achieves $\beta_N \approx 1.6$ and confinement factor $H_{98(y,2)} \approx 1.1$ relative to the IPB98(y,2) H-mode scaling [8]. However, even though the broadband MHD persists longer, in this case it appears inadequate to provide sufficient particle transport, density continues to rise, and ELMs eventually return. Shortly thereafter, a locked mode is encountered, similar to the high G plasmas at low torque. Clearly much more work is required to enable robust QH-mode access at low torque. Note that this example only used low levels of $n = 3$ fields; earlier attempts to try to maximize the $n = 3$ field had been less successful, in that the locked modes typically occurred even earlier.

Recent analysis has indicated that the challenges to low torque operation may in part be the result of a large $n = 1$ error field that is introduced together with the desired $n = 3$ field from the coils [9]. While the vacuum $n = 1$ field is very small, there is large amplification of this field in the plasma. Future experiments will investigate whether the limitation in low torque, low q_{95} QH-mode can be overcome with improved error field compensation.

3. Impurity transport driven by the EHO

Adequate transport of impurities is essential for maintaining a high fuel-ion ratio and high performance. In standard ELMing H-mode, impurity accumulation is avoided by the periodic particle expulsion from each ELM. However, since ELM mitigated or suppressed regimes are required for ITER to prevent excessive damage to plasma facing components, it is critical that any solution for the large heat fluxes associated with the ELMs be able to maintain adequate impurity transport.

Measurement of particle transport is complicated due to uncertainties in the particle

source terms, particularly due to recycling from the wall. Therefore, impurity transport measurements are best made using a species that is not typical in the tokamak and does not return to the plasma core. For these studies, carbon tetrafluoride (CF_4) was injected into the plasma, with charge exchange recombination (CER) spectroscopy measuring the F-IX (10-9) transition at 4796 Å. The impurity confinement time τ_P is readily determined from the exponential decay of the signal [10].

Figure 4 shows an example of the uptake and exhaust of F impurity following a 5 ms gas puff of CF_4. A database of discharges shows a dependence of the F impurity confinement time on the density for both QH-mode discharge and ELMing discharges. Importantly, one finds that at comparable densities, the QH-mode plasmas have impurity confinement times at least as short as regular ELMing plasmas with frequency about 40 Hz.

As previously noted, QH-mode plasmas exhibit increased energy confinement as the torque and rotation are reduced. Importantly, τ_P is found to be insensitive to the rotation, such that the ratio τ_P/τ_E actually decreases in the more reactor relevant range of low rotation (Fig. 4). Similar studies have also shown that τ_P is insensitive to the level of applied non-axisymmetric field [10].

4. Extension of QH-mode to ITER relevant densities

QH-mode has historically been associated with low density operation, and indeed, the general recipe for achieving robust QH-mode has been to work on limiting the fueling and reducing the density. While QH-mode operation is therefore associated with low collisionality as envisioned in a future reactor, the low normalized density associated with QH-mode has been an outstanding criticism about the applicability of the scenario to a device like ITER.

To address this long-standing issue, experiments were conducted to investigate the upper limits in density for QH-mode operation [11]. In particular, gas puffing was added during the QH-mode phase, controlled via density feedback to follow a pre-programmed ramping density target. In this way, the maximum tolerable density compatible with QH-mode was determined as indicated by the return of ELMs. An example of this is shown in Fig. 5, contrasted with typical QH-mode operation where little if any gas is puffed, a prescription that produces a strong EHO and the cleanest QH-mode performance.

Peeling-ballooning theory predicts that shaping should provide one of the strongest knobs for affecting the maximum tolerable density in QH-mode [12]. The EHO is believed to be the saturated state of a current-driven mode encountered along the kink-peeling boundary, for which rotation shear is destabilizing [12]. As such, operation

along the kink-peeling boundary is thought to be an essential requirement for access to QH-mode, and experimentally, plasmas with an EHO are always found to exist along this boundary. At low triangularity, operation along the kink-peeling boundary is only possible at very low densities, with higher density and collisionality driving the plasma toward the ballooning boundary. With stronger shaping, the stability boundary is calculated to widen, allowing QH-mode operation at higher densities.

Experiments have confirmed that stronger shaping allows higher density QH-mode in a scan of the minimum in the upper and lower triangularity of the plasma shape, $\delta \equiv \min(\delta_{\text{upper}}, \delta_{\text{lower}})$, with other key parameters such as toroidal field and plasma current and heating power held constant (Fig. 6). This data shows that plasmas with high triangularity can sustain QH-mode at double the Greenwald fraction of plasmas with reduced triangularity (here, the Greenwald fraction is $\bar{n}_e/n_G > 0.7$, where $n_G = I_p/\pi a^2$ is the Greenwald density limit for tokamaks [13]). This demonstrates that low density is not an inherent requirement for QH-mode operation.

With strong shaping, the QH-mode pedestal height is found to evolve to levels comparable with some of the highest performance transient pedestals seen on DIII-D. At fixed β_N, maintained with β_N feedback control of the neutral beam power, the height, width and gradient of the pedestal pressure all increase as the density increases, as shown in Fig. 7, and the increase in the density originates from the pedestal rather than via a central peaking of the density profile.

Examples of the measured profiles and their fits are shown in Fig. 8. Here, the total pressure is estimated as the contribution from the sum of the electron and ion pressures, together with a contribution from the beam ions (calculated with ONETWO/NUBEAM). One sees the significant range in pedestal density over which QH-mode conditions are maintained. Note that the pedestal temperature decreases, although by a lesser amount than the rise in density, such that the overall pressure increases with density.

Calculations of the expected pedestal evolution from EPED [14] are quantitatively consistent with the experimental measurements [11]. Similar EPED calculations using the ITER shape and other expected parameters find that the ITER pedestal will operate on the kink-peeling boundary where QH-mode can exist for all pedestal densities up to values exceeding 10^{20} m^{-3}, which is significantly higher than the baseline ITER $Q = 10$ scenario requirement [15].

5. Access to Super H-mode

Application of the EPED model has revealed that a second region of ELM-stable operation is possible in strongly shaped plasmas at high density, characterized by very

high pedestals. This new regimes has been dubbed "Super H-mode" [16]. Realizing this high pedestal state is a challenge because at fixed density, the plasma will encounter the lower pedestal solution first, preventing access to the high pedestal pressures predicted by EPED.

A time-evolving density trajectory in QH-mode, shown in Fig. 9, appears to have overcome this problem and accessed the Super H-mode regime [11]. For pedestal densities above approximately 6×10^{19} m^{-3}, EPED finds two separate regions for ELM stable operation (Fig. 10). By first establishing QH-mode at low collisionality, it has been possible to traverse the kink-peeling boundary and enter the "channel" of high pedestal pressure, avoiding the lower pedestal solution. Eventually, the plasma begins ELMing regularly, and the plasma exits the Super H-mode channel and down to the lower pedestal solution, resulting in nearly a factor of two reduction in the pedestal pressure with only a modest decrease in density. Therefore, the experimental trajectory in Fig. 10 demonstrates a bifurcation in the pedestal height at high density, as predicted by EPED.

The thermal energy confinement time is found to increase as the density and pedestal evolve to higher values, as seen in Fig. 11(a). Here, the thermal energy confinement time is computed from the measured density and temperature profiles and the neutral beam power and fast ion energy content calculated with TRANSP [17]. The confinement time rises more than 50% before a $m/n = 3/2$ tearing mode is destabilized and impacts the core confinement. The increasing thermal energy confinement would be expected in a plasma with an increasing pedestal height but stiff core transport. Indeed, the total thermal stored energy increases, owing to contributions from both the pedestal and core [Fig. 11(b)]. Therefore, the strong gas puffing used to fuel the plasma and raise the pedestal pressure does not lead to a degradation of core confinement. More detailed transport analysis confirms that the core thermal transport is even slightly reduced. Calculations with the transport model TGLF at various times during the density ramp also shows that the core transport is relatively stiff, and the thermal diffusivities are essentially constant independent of the pedestal (Fig. 12).

Although there is a significant improvement in the thermal energy confinement, the confinement factor $H_{98(y,2)}$ remains disappointingly constant as the pedestal rises. At first, this seems counterintuitive; one might expect the H-factor to increase if the thermal stored energy increases without the need of additional heating power. However, the IPB98(y,2) scaling already contains a strong density dependence ($n_e^{0.41}$), that appears to capture the increase in thermal energy confinement. To verify this, TRANSP simulations were performed, where profiles from the early QH-mode phase from Fig. 10 were used as the starting point, and then the pedestal density was increased monotonically to very

high values (well beyond that achieved in the experiment), with the pedestal pressure constrained according to the EPED solution and set as the boundary condition. At fixed power, the core profiles were then predicted, assuming constant diffusivity profiles. The results are shown in Fig. 13. Note that the plasma pressure profile becomes considerably broader at higher density and higher pedestal. One sees that the resultant computed $H_{98(y,2)}$ remains essentially constant over the entire density variation, despite the thermal energy and confinement increasing. Thus Super H-mode is not inherently a path to higher H-factors than typical H-mode. However, it does provide a path for maintaining H-mode levels of confinement at very high density, where standard H-mode typically deviates significantly from the IPB(98,y2) scaling.

The return of ELMs may be related to the loss of rotation shear [18], rather than an inherent transition from the current-driven kink-boundary to the pressure-driven ballooning-boundary. Reduced rotation and rotation shear arises due to the reduction in the injected torque per particle as the density increases, together with an increase in the co-current directed intrinsic torque [19, 20] as the pedestal gradients increase, which opposes the counter rotation driven by the counter-current beams used in these experiments. More detailed analysis has found that the shear in $\omega_E = E_r/RB_\theta$, the rotation driven by the radial electric field E_r may be the relevant quantity for QH-mode. As shown in Fig. 14, the shear in ω_E is found to be already below the empirical boundary described in Ref. [6] when the ELMs return.

Experiments have begun to try to exploit the enhanced Super H-mode pedestal by coupling it with a high performance core. In these plasmas, the global β_N was programmed to rise with the pedestal, as shown in Fig. 15. In these experiments, plasmas with $H_{98(y,2)} > 1.2$, $\beta_{N,ped} \approx 1.2$, and $\beta_N > 3$ have been obtained, which represents the highest β_N achieved with a quiescent edge to date. Typical of all higher β Super H-mode attempts, there is a competition between the transport from the EHO and the need to go to higher pedestal density. One sees dramatic changes in the pedestal density evolution as the EHO mode number and intensity changes, and in fact the Super H-mode regime is reached when the coherent EHO abruptly ends and is replaced with broadband MHD that exhibits less efficient particle transport [21]. Therefore, fully exploiting this regime requires careful balancing of the fueling and the EHO driven transport: too strong an EHO keeps the pedestal density down, while too weak an EHO is insufficient to prevent an ELM, leading to the exit of the Super H-mode channel.

Fig. 16 shows a comparison between the experimental pedestal parameters with EPED model predictions for a similar high β_N Super H-mode discharge. These higher β variants of Super H-mode do not move further into Super H-mode than the earlier modest β ones, and the challenge remains how to move deep into the Super H regime and

stay there, since unlike an L-H transition, the real advantage realized in Super H-mode is a function of how far up the improved stability channel one successfully navigates.

6. Conclusions

Recent experimental work in QH-mode suggests that it may be the most attractive operating scenario for succeeding in ITER's Q=10 mission. It exhibits inherently ELM-stable operation at ITER relevant values of β_N, H_{89}, q_{95}, torque and density, while maintaining adequate impurity exhaust. In addition, it has provided access to a new regime of very high pedestals called "Super H-mode", which if successfully exploited may open the path to much higher performance than currently achievable in standard H-mode.

This material is based upon work supported by the U.S. Department of Energy, Office of Science, Office of Fusion Energy Sciences, using the DIII-D National Fusion Facility, a DOE Office of Science user facility, under Awards DE-FC02-04ER54698, DE-AC02-09CH11466, DE-AC52-07NA27344, DE-FG02-89ER53296, DE-FG02-08ER54999 and DE-FG02-95ER54309. The views and opinions expressed herein do not necessarily reflect those of the ITER Organization.

[1] M. Shimada *et al.*, Nucl. Fusion **47**, S1 (2007).
[2] H. Zohm, Plasma Phys. Control. Fusion **38**, 105 (1996).
[3] A. Loarte *et al.*, Plasma Phys. Control. Fusion **45**, 1549 (2003).
[4] K.H. Burrell *et al.*, Phys. Plasmas **8**, 2153 (2001).
[5] D.G. Whyte *et al.*, Nucl. Fusion **50**, 105005 (2010).
[6] A.M. Garofalo *et al.*, Nucl. Fusion **51**, 083018 (2011).
[7] A.M. Garofalo *et al.*, Phys. Rev. Lett. **101**, 195005 (2008).
[8] ITER Physics Expert Groups on Confinement and Transport and Confinement Modelling and Database, ITER Physics Basis Editors 1999 *Nucl. Fusion* **39** 2175
[9] A.M. Garofalo *et al.*, "The Quiescent H-mode Regime for High Performance ELM-Stable Operation in Future Burning Plasmas", to be submitted to Phys. Plasmas (2015).
[10] B.A. Grierson *et al.*, Nucl. Fusion **54**, 114011 (2014).
[11] W.M. Solomon *et al.*, Phys. Rev. Lett. **113**, 135001 (2014).
[12] P.B. Snyder *et al.*, Nucl. Fusion **47**, 961 (2007).
[13] M. Greenwald, Plasma Phys. Control. Fusion **44**, R27 (2002).
[14] P.B. Snyder *et al.*, Phys. Plasmas **16**, 056118 (2009).
[15] K.H. Burrell *et al.*, Phys. Plasmas **19**, 056117 (2012).
[16] P.B. Snyder *et al.* Proc. 24th Int. Conf. (San Diego, USA, 2012) (Vienna: IAEA) CD-ROM file th_p3-17.pdf and http://www-naweb.iaea.org/napc/physics/FEC/FEC2012/html/fec12.htm
[17] R.J. Hawryluk, in *Phys. Plasmas Close to Thermonuclear Conditions*, edited by B. Coppi *et al.* (CEC, Brussels, 1980), Vol. 1, pp. 19-46.
[18] K.H. Burrell *et al.*, Phys. Rev. Lett. **102**, 155003 (2009).
[19] W.M. Solomon *et al.*, Phys. Plasmas **17**, 056108 (2010).
[20] W.M. Solomon *et al.*, Nucl. Fusion **51**, 073010 (2011).
[21] B.A. Grierson *et al.*, "Impurity confinement and transport in high confinement regimes without ELMs on DIII-D", submitted to Phys. Plasmas (2014).

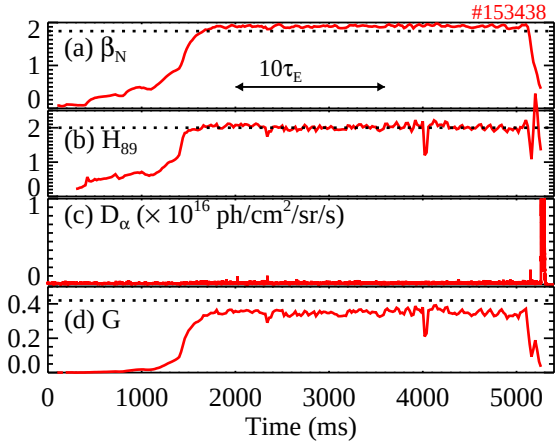

Figure 1. High performance QH-mode: (a) β_N; (b) H_{89} factor; (c) D_α brightness and; (d) normalized fusion performance $G = \beta_N H_{89}/q_{95}^2$.

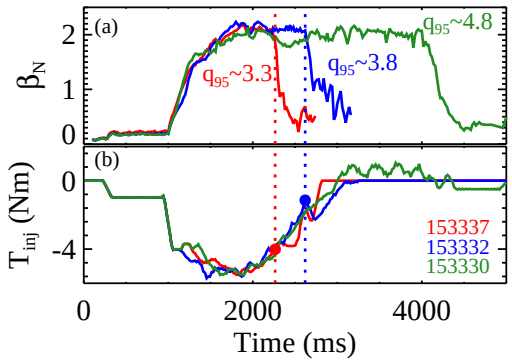

Figure 2. The torque required for stable operation is seen to increase as q_{95} decreases. (a) β_N, and (b) neutral beam torque. The approximate time of locking is indicated by the dashed curve for the lower q_{95} values and the corresponding torque at those times is also shown by the solid circles.

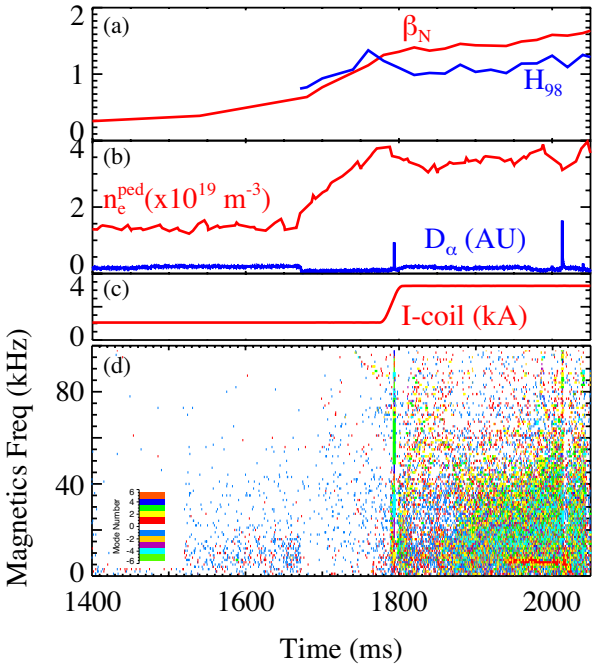

Figure 3. QH-mode with low torque startup. (a) β_N and H_{98}; (b) Pedestal density and D_α light; (c) I-coil current; (d) Spectrogram with toroidal modal number identification from magnetics measurements.

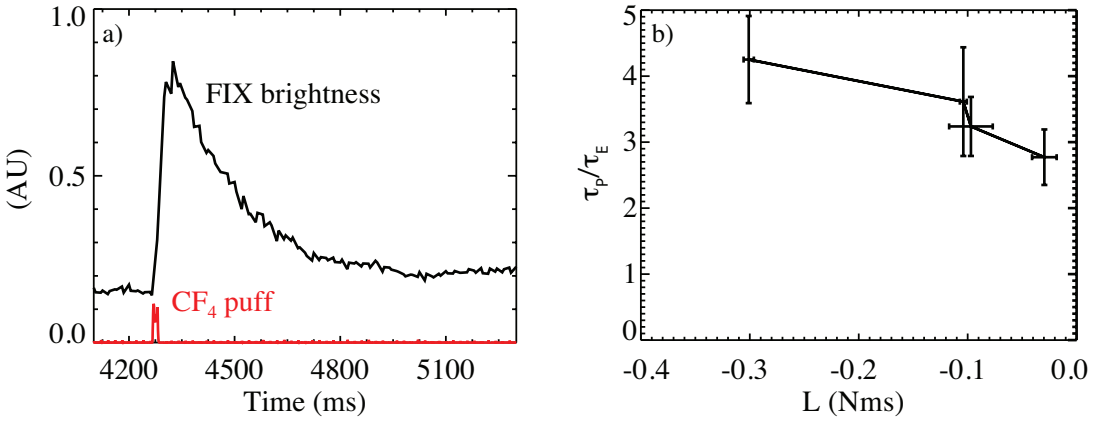

Figure 4. (a) F emission measured by CER following injection of CF_4. (b) Ratio of τ_P/τ_E as a function of the angular momentum in QH-mode plasmas, scanned here through controlled variation of the neutral beam torque.

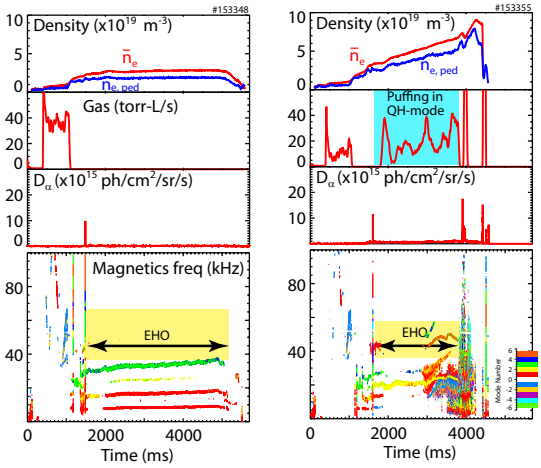

Figure 5. Density, gas, D_α light and magnetic spectrogram for typical QH-mode (left), and QH-mode with density ramp and strong gas puffing (right).

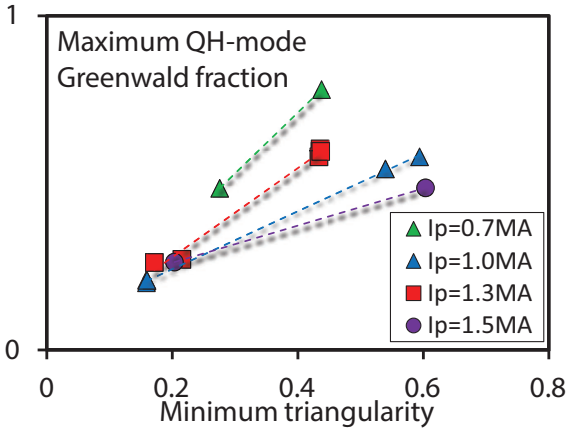

Figure 6. Maximum attainable QH-mode Greenwald fraction as a function of triangularity at fixed plasma current and toroidal field.

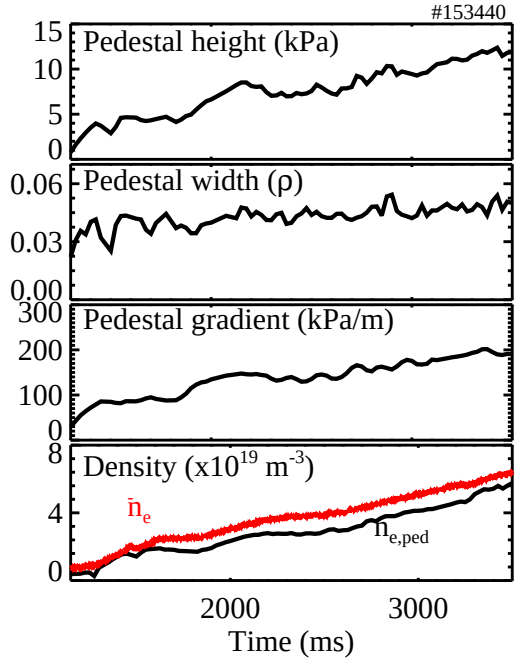

Figure 7. Evolution of QH-mode during density ramp by gas puffing.

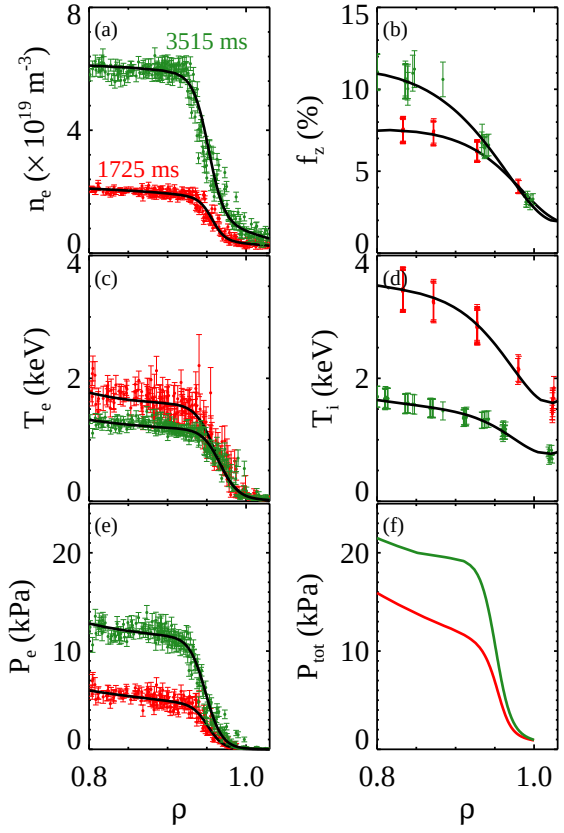

Figure 8. QH-mode pedestal profiles at low (red) and high (green) density: (a) electron density; (b) carbon concentration; (c) electron temperature; (d) ion temperature; (e) electron pressure; (f) total pressure.

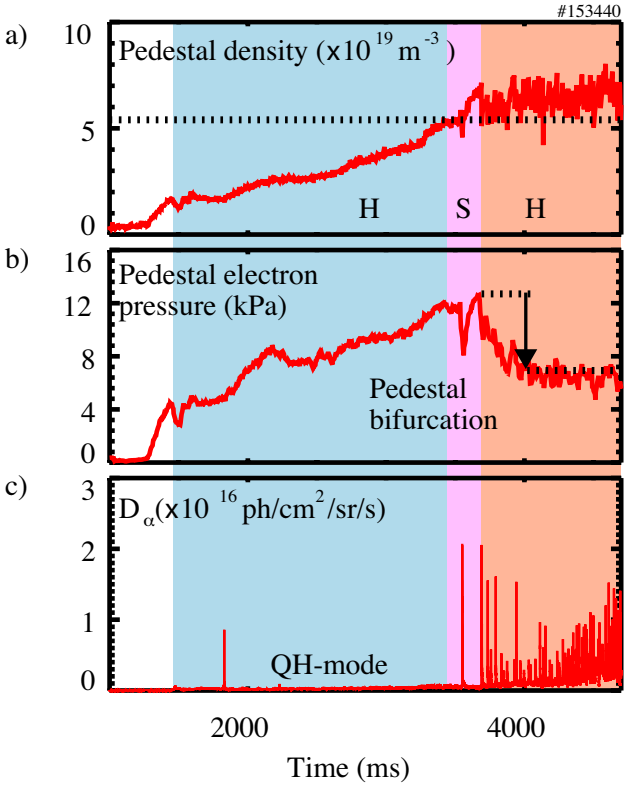

Figure 9. Time evolution of QH-mode plasma as density is raised with gas puffing: (a) Pedestal density; (b) Pedestal electron pressure; and (c) D_α brightness.

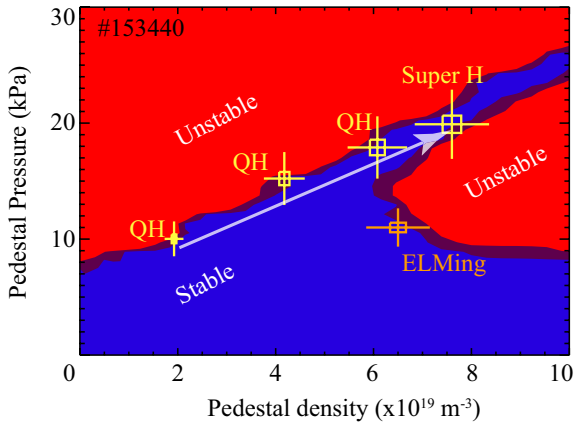

Figure 10. Experimental trajectory of QH-mode pedestal into predicted Super H-mode regime of high pedestal and bifurcation to lower pedestal ELMing state.

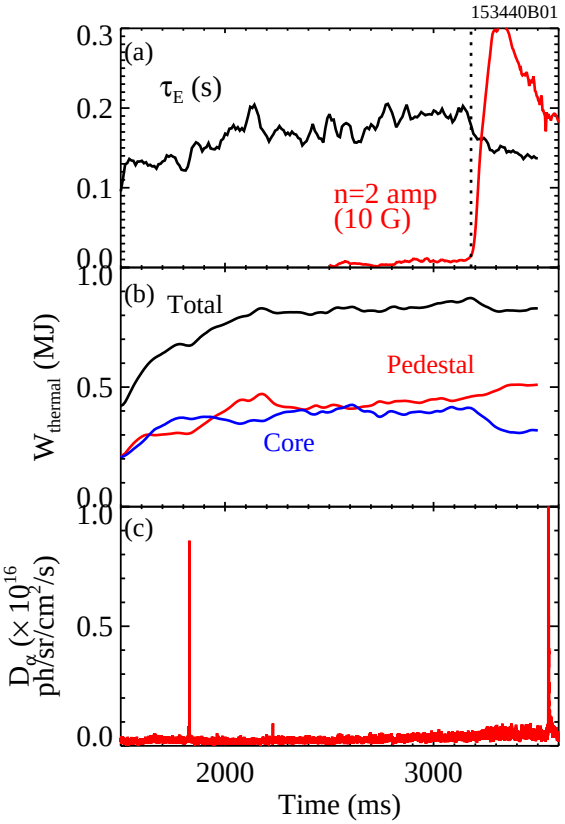

Figure 11. (a) Thermal energy confinement time and $n = 2$ amplitude; (b) thermal energy content; and (c) D_α light.

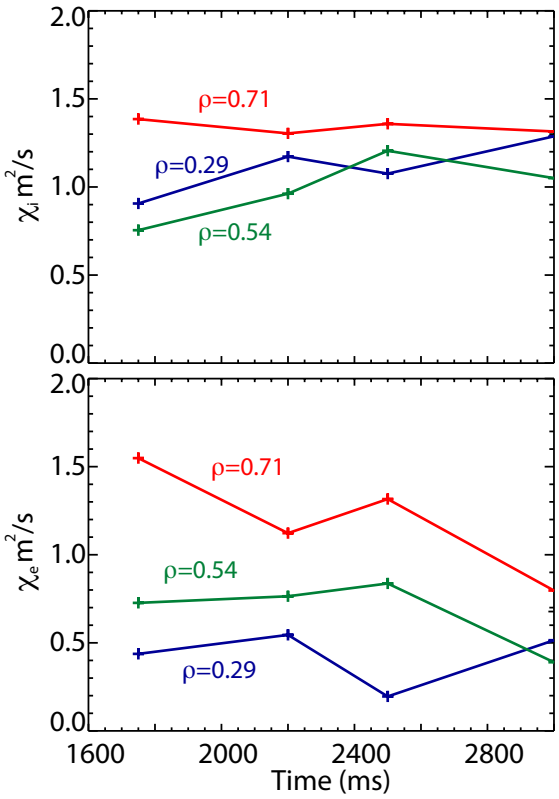

Figure 12. Time histories (corresponding to increasing density) of the ion and electron thermal diffusivities at different radii.

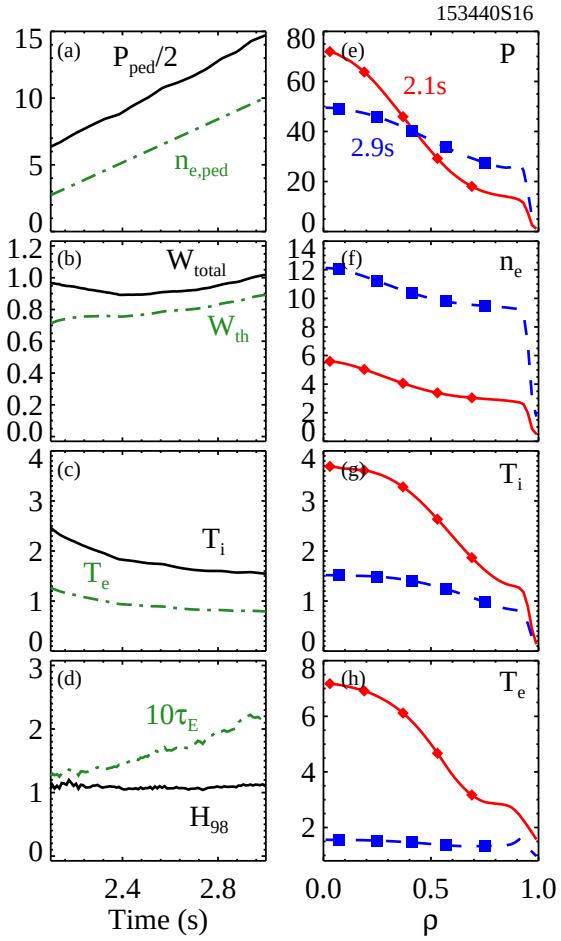

Figure 13. TRANSP simulation of increasing pedestal density with fixed thermal diffusivity following EPED solution. Time histories for: (a) Pedestal pressure (kPa) and pedestal density ($\times 10^{19}$ m^{-3}); (b) Total and thermal stored energy (MJ); (c) Ion and electron temperature (keV); (d) H_{98} and thermal energy confinement time (s). Profiles at low and high pedestal density, corresponding to 2.1 and 2.9 s in the simulation: (e) Plasma pressure (kPa); (f) electron density ($\times 10^{19}$ m^{-3}); (g) ion temperature (keV); and (h) electron temperature (keV).

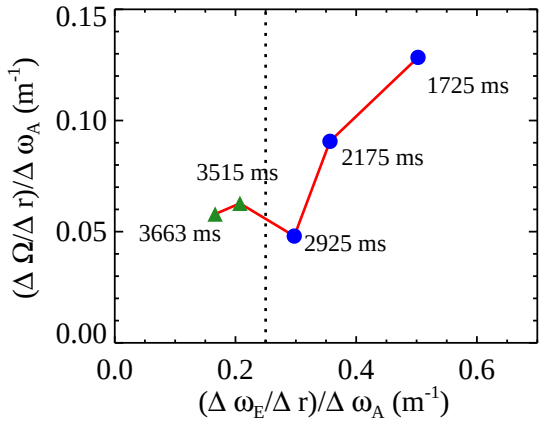

Figure 14. Edge shear of impurity rotation versus edge shear in ω_E at different times in the QH-mode to Super H-mode evolution. The empirical boundary established in Ref. [6] is indicated by the dashed line. Standard QH-mode is shown with blue circles, while the Super H periods are indicated by green triangles

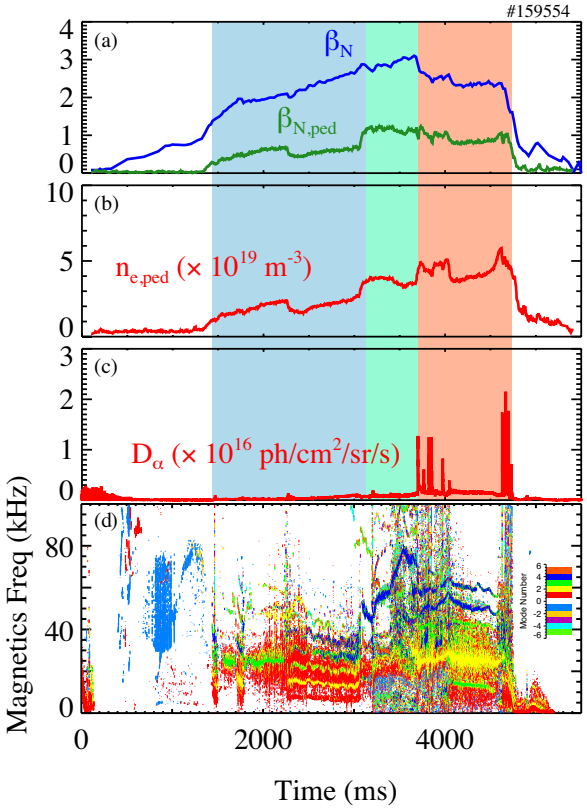

Figure 15. Super H-mode at higher β_N. (a) global and pedestal β_N ; (b) pedestal density; (c) D_α light; and (d) magnetic spectrogram. The period when the plasma is in the Super H channel is indicated with the shading.

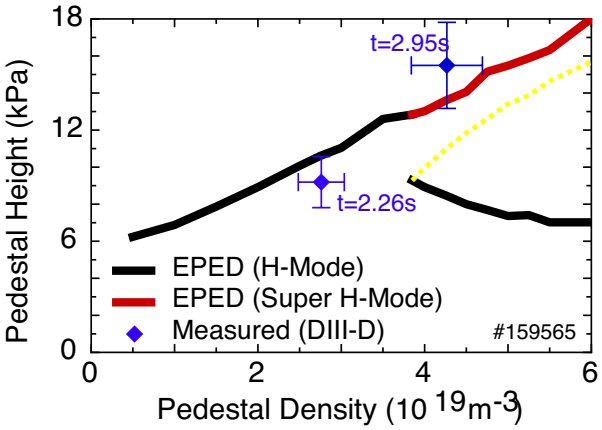

Figure 16. Comparison of EPED model predictions for the pedestal height versus pedestal density, compared with experimental measurements at two times, early in standard QH-mode and later in the Super H-mode channel.

Princeton Plasma Physics Laboratory
Office of Reports and Publications

Managed by
Princeton University

under contract with the
U.S. Department of Energy
(DE-AC02-09CH11466)

P.O. Box 451, Princeton, NJ 08543
Phone: 609-243-2245
Fax: 609-243-2751

E-mail: publications@pppl.gov
Website: http://www.pppl.gov